Appendix: Point-Cloud Method for Automated 3D Coronary Tree Reconstruction from Multiple Non-simultaneous Angiographic Projections

Abhirup Banerjee, Francesca Galassi, Ernesto Zacur, Giovanni Luigi De Maria, Robin P. Choudhury, and Vicente Grau

***Abstract*—X-ray angiography is the most commonly used imaging modality for the detection of coronary stenoses due to its high spatial and temporal resolution of lumen contour and its utility to guide coronary interventions in real time. However, the high inter- and intra-observer variability in interpreting the geometry of 3D vascular structure based on multiple 2D image projections is a limitation in the accurate determination of lesion severity. This could be addressed by the 3D reconstruction of the coronary arterial (CA) tree. The automated reconstruction of 3D CA tree from 2D projections is challenging due to the existence of several imaging artifacts, such as vessel overlap, foreshortening, and most importantly respiratory and cardiac motion. Along with these artifacts, the acquisition geometry introduces the possibility of generating false vessel segments in the reconstruction. Our approach aims to reduce the motion artifacts in angiographic projections by developing a new method for rigid and non-rigid motion correction. A novel point-cloud based approach is subsequently introduced for reconstruction of 3D vessel centerlines by iteratively minimizing the reconstruction error. The performance of the proposed 3D reconstruction is evaluated using angiographic projections from 45 patients, producing average reprojection errors of 0.092 ± 0.055 mm and 0.910 ± 0.352 mm for 3D centerlines reconstruction, when co-registered with the parent vessels on projection planes that were/were not used to derive the 3D reconstruction, respectively. A comparison of the reconstructed 3D lumen surface with optical coherence tomography (OCT) measurements has been performed, showing no statistically significant difference in the luminal cross-sections reconstructed with our method, compared to OCT.**

***Index Terms*—Point-cloud, 3D coronary tree reconstruction, 3D centerline reconstruction, motion correction, X-ray angiograms, optical coherence tomography.**

A. Banerjee is with the Radcliffe Department of Medicine, Division of Cardiovascular Medicine, University of Oxford, Oxford, United Kingdom and the Department of Engineering Science, Institute of Biomedical Engineering, University of Oxford, Oxford, United Kingdom. E-mail: abhirup.banerjee@cardiov.ox.ac.uk.

F. Galassi and R. P. Choudhury are with the Oxford Acute Vascular Imaging Centre, Oxford, United Kingdom and the Radcliffe Department of Medicine, Division of Cardiovascular Medicine, University of Oxford, Oxford, United Kingdom. E-mail: robin.choudhury@cardiov.ox.ac.uk.

E. Zacur and V. Grau are with the Department of Engineering Science, Institute of Biomedical Engineering, University of Oxford, Oxford, United Kingdom. E-mail: {ernesto.zacur,vicente.grau}@eng.ox.ac.uk.

G. L. De Maria is with the Oxford Heart Centre, National Institute for Health Research Biomedical Research Centre, Oxford University Hospitals, Oxford, United Kingdom. E-mail: GiovanniLuigi.DeMaria@ouh.nhs.uk.

This work was supported in part by British Heart Foundation (BHF) Project Grant (no. HSR00410). It was also supported by the NIHR Oxford Biomedical Research Centre and the BHF Centre of Research Excellence, Oxford.

Algorithm 1: Proposed Rigid Motion Correction

Input : Image frames at end-diastole from each projection plane
Output: Rigid motion corrected image frames

Select (manually) n vessel landmarks (preferably $4-6$) from all projection planes;
do
  Estimate the rigid motion corrected 3D landmarks as the nearest orthogonal point of 3D projection lines connecting vessel landmarks on projection planes with the source (using (1) and (3));
  Estimate the optimal rigid transformation for each acquisition so that the 3D landmarks match with rigid motion corrected landmarks (using (2));
while *the 3D landmarks for each image acquisition do not coincide*;
Return the optimal transformation that minimizes the effect of rigid motion.

I. Appendix

A. Derivation of Multiple Solutions from Point Correspondences Between Angiographic Projections

$$
\begin{aligned}
& f_1(y_1) = f_2(y_2) \\
i.e. \quad & S_1 + d_1 \frac{(M_1 - S_1).N_1}{(A(y_1) - S_1).N_1}(A(y_1) - S_1) = \\
& \qquad S_2 + d_2 \frac{(M_2 - S_2).N_2}{(A(y_2) - S_2).N_2}(A(y_2) - S_2) \\
i.e. \quad & \left(\frac{(M_1 - S_1).N_1}{(A(y_1) - S_1).N_1}(A(y_1) - S_1) \right. \\
& \left. - \frac{(M_2 - S_2).N_2}{(A(y) - S_2).N_2}(A(y) - S_2) \quad (S_1 - S_2) \right) \begin{pmatrix} d_1 \\ d_2 \\ 1 \end{pmatrix} = 0 \\
i.e. \quad & \left| \frac{(M_1 - S_1).N_1}{(A(y_1) - S_1).N_1}(A(y_1) - S_1) \right. \\
& \left. - \frac{(M_2 - S_2).N_2}{(A(y) - S_2).N_2}(A(y) - S_2) \quad (S_1 - S_2) \right| = 0 \\
& \text{since} \quad d_1, d_2 \neq 0
\end{aligned}
$$

$$
\begin{aligned}
i.e. \quad & |(A(y_1)-S_1) \quad (A(y)-S_2) \quad (S_1-S_2)| = 0 \\
& \text{since} \quad \frac{(M_1-S_1).N_1}{(A(y_1)-S_1).N_1}, \frac{(M_2-S_2).N_2}{(A(y)-S_2).N_2} \neq 0 \\
i.e. \quad & \left| R\begin{pmatrix} y_1^2 \\ ay_1 \\ 0 \end{pmatrix} - S_1 \quad R\begin{pmatrix} y_2^2 \\ ay_2 \\ 0 \end{pmatrix} - S_2 \quad S_1 - S_2 \right| = 0 \\
& \left[R = \frac{1}{a} R(\text{say}), |R| \neq 0 \right] \\
i.e. \quad & \left| \begin{pmatrix} y_1^2 \\ ay_1 \\ 0 \end{pmatrix} - R^{-1}S_1 \quad \begin{pmatrix} y_2^2 \\ ay_2 \\ 0 \end{pmatrix} - R^{-1}S_2 \; R^{-1}(S_1-S_2) \right| = 0 \\
i.e. \quad & \begin{vmatrix} y_1^2 - (R^{-1}S_1)_1 & y_2^2 - (R^{-1}S_2)_1 & \\ ay_1 - (R^{-1}S_1)_2 & ay_2 - (R^{-1}S_2)_2 & R^{-1}(S_1-S_2) \\ -(R^{-1}S_1)_3 & -(R^{-1}S_2)_3 & \end{vmatrix} = 0 \\
i.e. \quad & \begin{vmatrix} y_1^2 - (R^{-1}S_1)_1 & y_2^2 - y_1^2 & \\ ay_1 - (R^{-1}S_1)_2 & ay_2 - ay_1 & R^{-1}(S_1-S_2) \\ -(R^{-1}S_1)_3 & 0 & \end{vmatrix} = 0 \\
& [C_2 = C_2 - C_1 - C_3] \\
i.e. \quad & \begin{vmatrix} y_1^2 - (R^{-1}S_1)_1 & y_2 + y_1 & (R^{-1}S_1)_1 - (R^{-1}S_2)_1 \\ ay_1 - (R^{-1}S_1)_2 & a & (R^{-1}S_1)_2 - (R^{-1}S_2)_2 \\ -(R^{-1}S_1)_3 & 0 & (R^{-1}S_1)_3 - (R^{-1}S_2)_3 \end{vmatrix} \\
& (y_2 - y_1) = 0 \\
i.e. \quad & y_2 = y_1 \\
\text{or} \quad & -ay_1y_2((R^{-1}S_1)_3 - (R^{-1}S_2)_3) + (y_2+y_1) \\
& ((R^{-1}S_1)_3(R^{-1}S_2)_2 - (R^{-1}S_1)_2(R^{-1}S_2)_3) \\
& -a((R^{-1}S_1)_3(R^{-1}S_2)_1 - (R^{-1}S_1)_1(R^{-1}S_2)_3) = 0 \\
i.e. \quad & -ay_1y_2Q_1 + (y_2+y_1)Q_2 - aQ_3 = 0 \\
i.e. \quad & y_2 = \frac{aQ_3 - y_1Q_2}{Q_2 - ay_1Q_1} \\
\text{where} \quad & Q_1 = (R^{-1}S_1)_3 - (R^{-1}S_2)_3 \\
& Q_2 = (R^{-1}S_1)_3(R^{-1}S_2)_2 - (R^{-1}S_1)_2(R^{-1}S_2)_3 \\
\text{and} \quad & Q_3 = (R^{-1}S_1)_3(R^{-1}S_2)_1 - (R^{-1}S_1)_1(R^{-1}S_2)_3.
\end{aligned}
$$

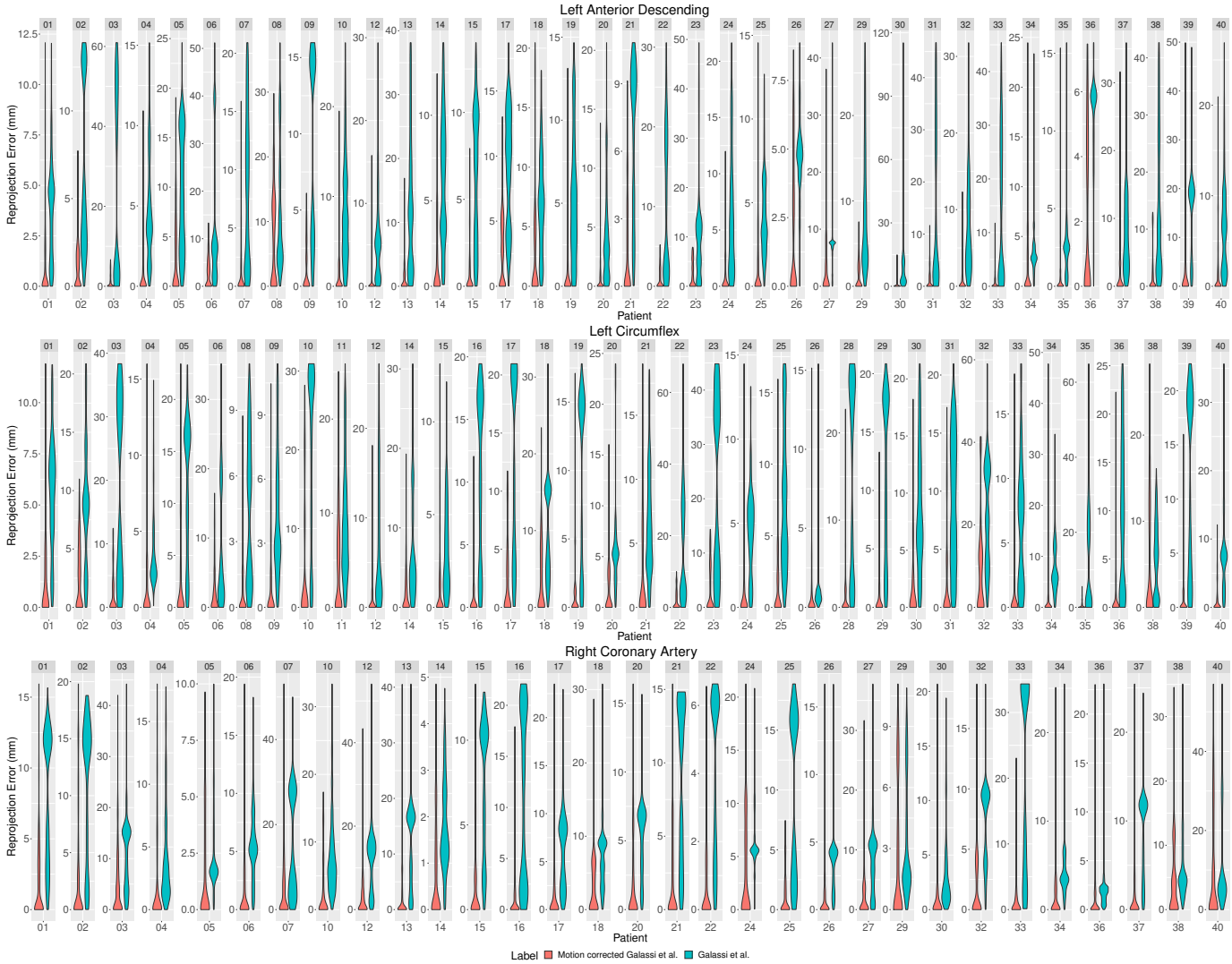

Fig. 1: Comparison between reprojection errors, measured after back-projecting the reconstructed 3D centerlines as in Galassi et al., with and without the rigid motion correction

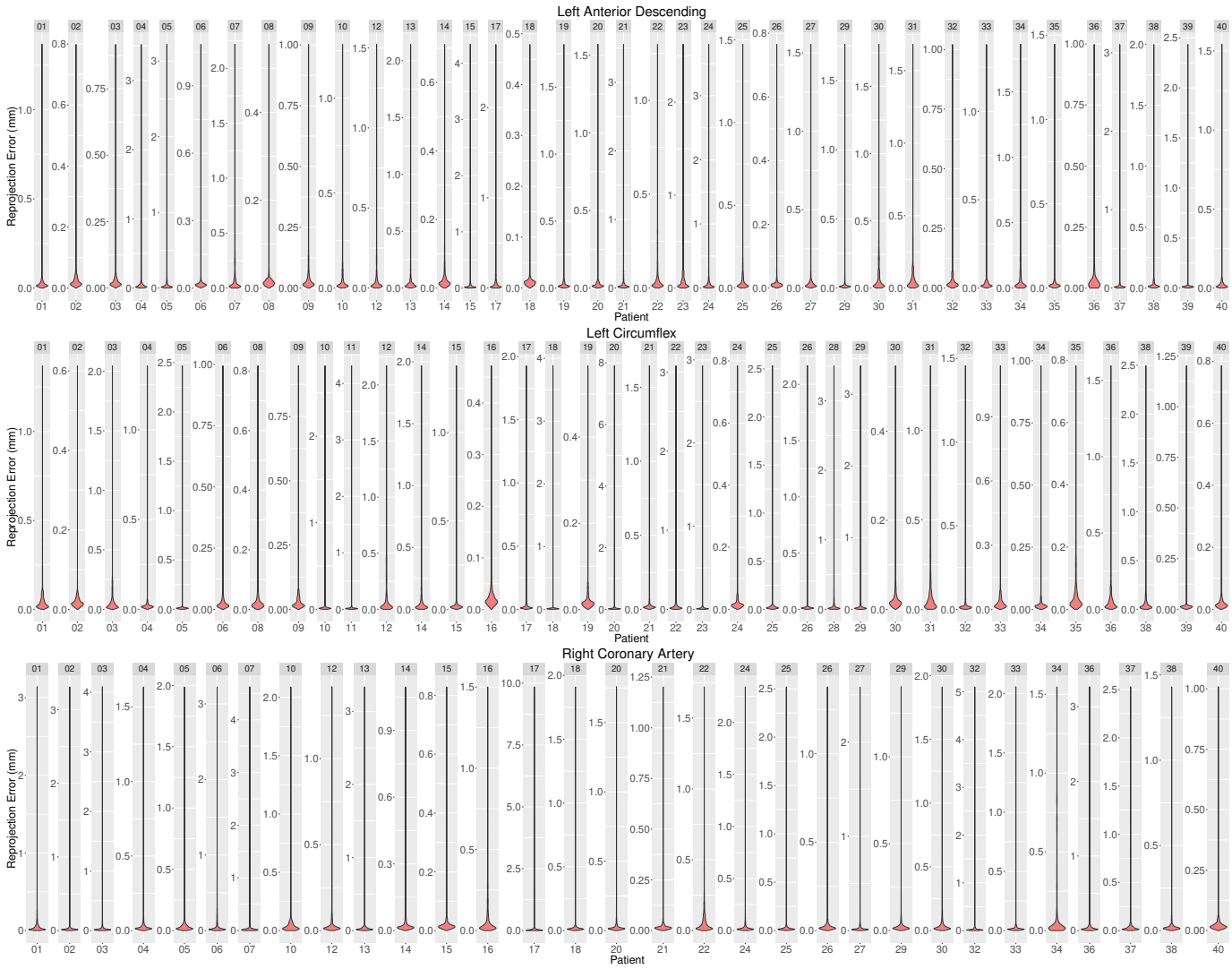

Fig. 2: Evaluating the reprojection errors after 3D centerlines reconstruction.

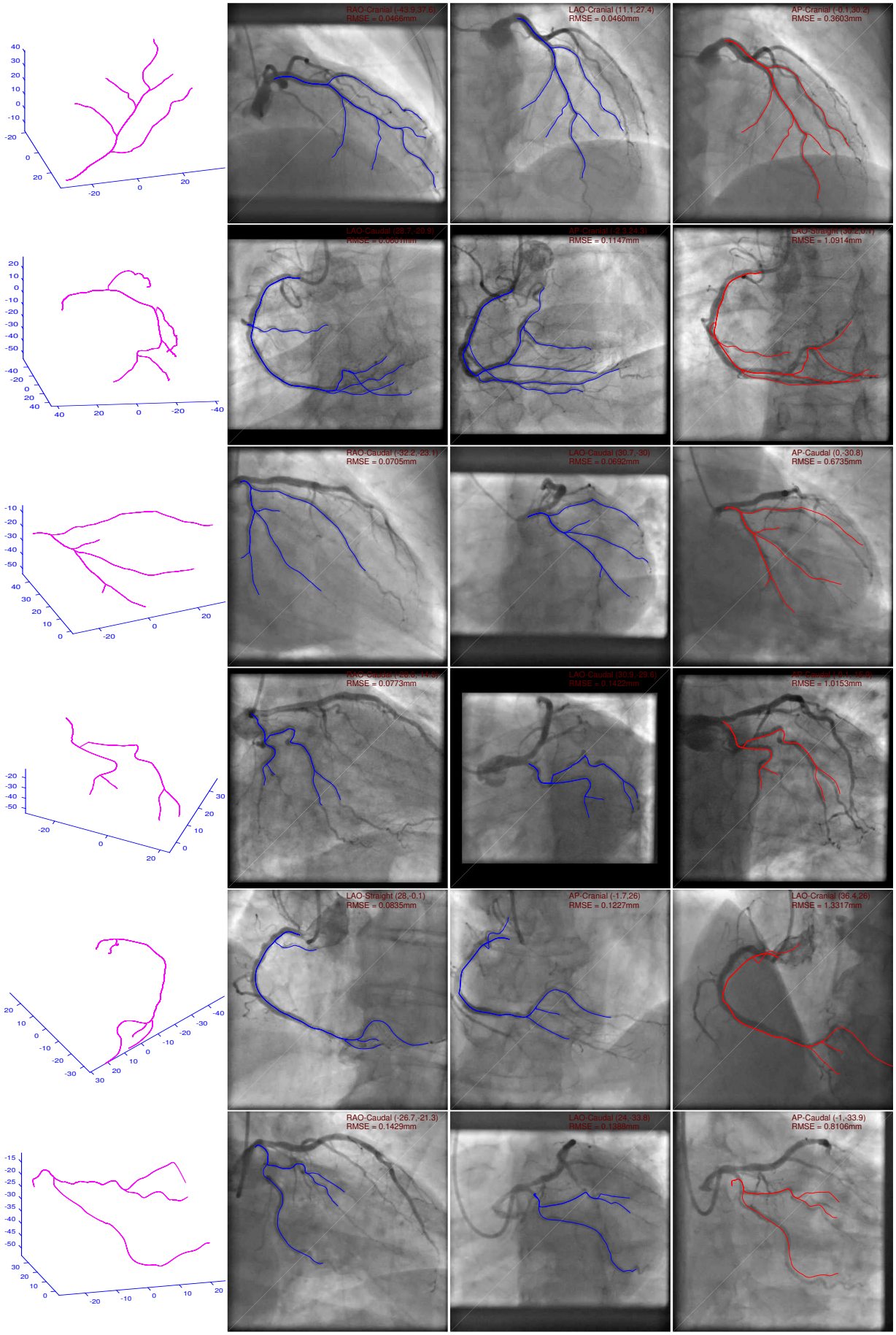

Fig. 3: Left to right: reconstructed 3D centerlines by proposed approach, the reprojections of 3D centerlines on two original angiographic planes, and the reprojection on an additional angiographic plane, not used for reconstruction. Top to bottom: Patient 2-LAD, 3-RCA, 7-LCx, 15-LCx, 18-RCA, and 20-LCx.

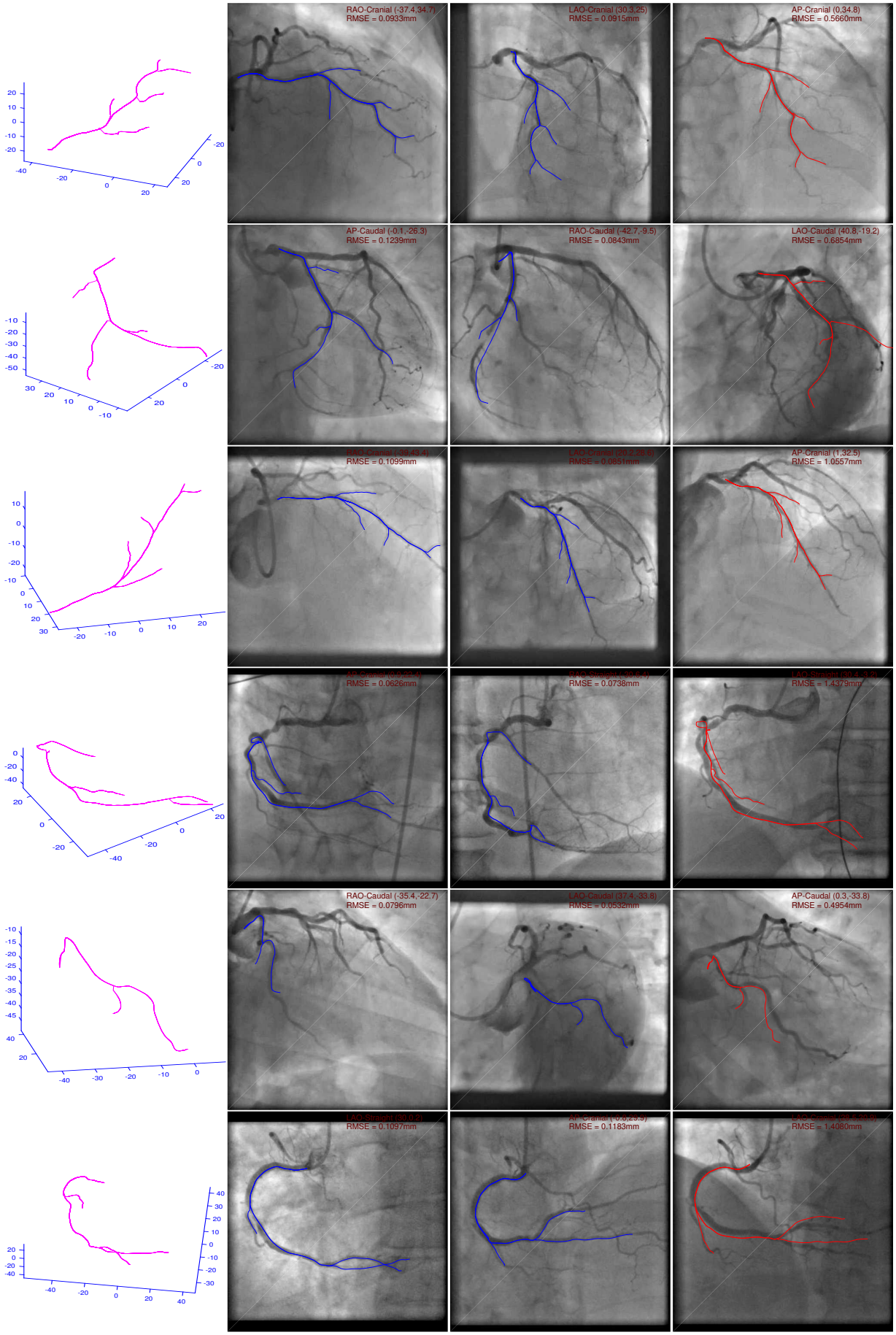

Fig. 4: Left to right: reconstructed 3D centerlines by proposed approach, reprojections of 3D centerlines on two original angiographic planes, and the reprojection on an additional image plane, not used for reconstruction. Top to bottom: Patient 25-LAD, 26-LCx, 35-LAD, 40-RCA, 46-LCx, and 56-RCA.